

Dynamical energy analysis—Determining wave energy distributions in vibro-acoustical structures in the high-frequency regime

Gregor Tanner*

School of Mathematical Sciences, University of Nottingham, University Park, Nottingham NG7 2RD, UK

Received 10 April 2008; received in revised form 27 July 2008; accepted 28 August 2008

Handling Editor: C.L. Morfey

Available online 14 October 2008

Abstract

We propose a new approach towards determining the distribution of mechanical and acoustic wave energy in complex built-up structures. The technique interpolates between standard *statistical energy analysis* (SEA) and full *ray tracing* containing both these methods as limiting cases. By writing the flow of ray trajectories in terms of linear phase space operators, it is suggested to reformulate ray-tracing algorithms in terms of boundary operators containing only short ray segments. SEA can now be identified as a low resolution ray-tracing algorithm and typical SEA assumptions can be quantified in terms of the properties of the ray dynamics. The new technique presented here enhances the range of applicability of standard SEA considerably by systematically incorporating dynamical correlations wherever necessary. Some of the inefficiencies inherent in typical ray-tracing methods can be avoided using only a limited amount of the geometrical ray information. The new dynamical theory—*dynamical energy analysis* (DEA)—thus provides a universal approach towards determining wave energy distributions in complex structures in the high-frequency limit.

© 2008 Elsevier Ltd. All rights reserved.

1. Introduction

Wave energy distributions in complex mechanical systems can often be modelled well by using a thermodynamical approach. Lyon argued as early as 1967 [1] that the flow of wave energy follows the gradient of the energy density just like heat energy flows along the temperature gradient. To simplify the treatment, it is often suggested to partition the full system into subsystems and to assume that each subsystem is internally in ‘thermal’ equilibrium. Interactions between directly coupled subsystems can then be described in terms of coupling constants determined by the properties of the wave dynamics at subsystem boundaries alone. These ideas form the basis of *statistical energy analysis* (SEA) which has become an important tool in mechanical engineering and has been described in detail in text books by Lyon and DeJong [2], Keane and Price [3] and Craik [4].

*Tel.: +44 115 9513842.

E-mail address: gregor.tanner@nottingham.ac.uk

A method similar in spirit but very different in applications is the so-called *ray-tracing technique*. The wave intensity distribution at a specific point r is determined here by summing over contributions from all ray paths starting at a source point r_0 and reaching the receiver point r . It thus takes into account the full flow of ray trajectories. The method has found widespread applications in room acoustics [5] and seismology [6] as well as in determining radio wave field distributions in wireless communication [7] and in computer imaging software [8]. A discussion of ray-tracing algorithms used for analysing the energy distribution in vibrating plates can be found in Refs. [9,10].

Both methods—that is, SEA and ray tracing—are in fact complementary in many ways. Ray tracing can handle wave problems well, in which the effective number of reflections at walls or interfaces is relatively small. It gives estimates for the wave energy density with detailed spatial resolution and works for all types of geometries and interfaces. SEA can deal with complex structures carrying wave energy over many subelements including potentially a large number of reflections and scattering events albeit at the cost of reduced resolution. In addition, the quality of SEA predictions may depend on how the subsystems are chosen as well as on the geometry of the subsystems itself, and error bounds are often hard to obtain.

Ray tracing and SEA have in common that they predict mean values of the energy distribution and do not contain information about wave effects such as interference, diffraction or tunnelling giving rise to modulations of the signal on the scale of a wavelength. Both methods are thus expected to hold in the high-frequency or small wavelength limit where the small scale fluctuations in the wave solutions are often averaged out, for example, due to a finite resolution of the receiver.

It will be shown here that SEA can be derived from a ray picture and is indeed a low resolution version of a ray-tracing method. Ray tracing is thus superior to SEA, however, at a large computational overhead. This observation has also been made in a numerical study by Kulkarni et al. [10]. We introduce a new technique here which interpolates between SEA and a full ray-tracing analysis. The method—called *dynamical energy analysis* (DEA)—keeps as much information about the underlying ray dynamics as necessary, benefiting at the same time from the simplicity of the SEA ansatz. DEA is thus an SEA type method in spirit but enhances the range of applicability of standard SEA considerably and makes it possible to give quantitative error bounds for an SEA treatment.

The ideas as presented here have their origin in wave or quantum chaos theory in which short wavelength approximations are combined with dynamical systems or chaos theory, see [11] for an overview. Methods similar in spirit to the theory outlined in this paper have been discussed in the context of structural dynamics before. Heron [12] modelled correlations between energy densities in subsystems which are not adjacent to each other in terms of direct and indirect contributions; the method does not take into account the actual ray dynamics and thus neglects long range dynamical correlations. Langley's [13,14] *wave intensity analysis* (WIA) treats the wave field within each subcomponent as an (inhomogeneous) superposition of plane waves thus introducing directionality which can propagate across coupling boundaries. The wave field is, however, assumed to be spatially homogeneous in each subsystem—an ad hoc assumption which may often not be fulfilled. In a ray-tracing treatment developed in a series of papers by Le Bot [15–17], a Green function for the mean energy flow is obtained from local power balance equations, and the full flow across subsystems is obtained via flux conditions. The approach presented here differs in as far as we consider multi-reflection in terms of linear operators directly and use a basis function representation of these operators leading to SEA-type equations.

The paper is structured as follows: in Section 2, we will briefly review the ideas behind standard SEA. In Section 3 the ray-tracing approximation will be derived starting from the Green function and using small wavelength asymptotics. In Section 4, we will introduce the concept of phase space operators and their representation in terms of boundary basis functions. SEA emerges when restricting the basis set to constant functions only. A specific example—coupled two plate system will be treated in Section 5.

2. SEA revisited

The starting point for an SEA treatment is the division of the whole system into subsystems; this is usually done along natural boundaries, such as joints between plates or walls in a building. Energy is pumped into the system at localised or delocalised source points (such as the vibrations of a motor) and is distributed

throughout the systems in terms of vibrational or acoustic energy in one form or another. The net power flow between subsystems is then given in the simple form

$$P_{ij} = \omega n_i \eta_{ij} \left(\frac{E_i}{n_i} - \frac{E_j}{n_j} \right), \quad (1)$$

where P_{ij} is the power transmitted between subsystem j and i , ω is the (mean) frequency of the source, n_i is the modal density of the (uncoupled) subsystem i (with respect to frequency), η_{ij} is a coupling constant and E_i is the total vibrational energy in subsystem i . Allowing for a source term and dissipation and getting estimates for the coupling constants [2,18,19] and the modal densities via Weyl's law, one obtains a linear systems of equations which is solved for the unknown energies E_i . SEA gives mean values for these energies in the same way as Weyl's law gives the mean density of eigenfrequencies.

The validity of Eq. (1) is based on various assumptions which can be summarised in the following way: (i) it is assumed that subsystems have no memory, that is, the coupling constants η_{ij} depend on the properties of subsystems i and j alone and (ii) the eigenfunctions of the (uncoupled) subsystems are expected to be locally described in terms of random Gaussian fields ('diffusive wave fields'). These two key assumptions are expected to be valid only in the high-frequency regime, for low absorption and for weakly coupled subsystems having 'irregular' shape [19,20]. The validity of these assumptions is often hard to control compromising the predictive capability of SEA. The method presented in the next sections can overcome this problem in principle, by reintroducing correlation effects as well as lifting the prerequisite that the wave and ray dynamics in each subsystem is in a quasi 'equilibrium state' with uniform distributions across the subsystem. Connections between SEA and the dynamical properties of the flow of ray trajectories has so far been made only indirectly. The statistical properties of wave systems with a chaotic classical ray dynamics have been shown to follow random matrix theory with wave functions behaving like random Gaussian waves [21]. The basic SEA assumptions thus imply that the ray dynamics in each subelement needs to be chaotic. This point of view has been stressed in the SEA literature by Weaver [22] and more recently in the context of determining the variance of the wave output data in Refs. [23–26]. A detailed review discussing the connections between ray and wave chaos has been given by Tanner and Søndergaard [11].

3. Wave energy density—from the Green function to the diagonal approximation

3.1. The Green function

We assume that the system as a whole is characterised by a linear wave operator \hat{H} describing the overall wave dynamics, that is, the motion of all coupled subcomponents as well as damping and radiation. In the case of acoustic pressure waves in homogeneous media, we have, for example, $\hat{H} = -c^2 \Delta$, where c is the wave velocity. Different types of wave equations may be used in different parts of the system typically ranging from the Helmholtz equation for thin membranes and acoustic radiation to the biharmonic equation for plate-like elements and to vector wave equations describing in-plane modes in plates and bulk elasticity in isotropic or anisotropic media. We restrict the treatment here to stationary problems with continuous, monochromatic energy sources—generalising the results to the time domain with impulsive sources is straightforward.

To simplify the notation, we will in the following assume that \hat{H} is a scalar operator; treating bulk elasticity does not pose conceptual problems and follows for isotropic problems from Ref. [27] and for the anisotropic case, for example, from Ref. [28]. Note that both in SEA as in the new method—DEA—developed below, different wave modes such as pressure, shear or bending waves will be treated as different subsystems.

The general problem of determining the response of a system to external forcing can then be reduced to solving

$$(\omega^2 - \hat{H})G(r, r_0, \omega) = \frac{F_0}{\mu} \delta(r - r_0), \quad (2)$$

where the Green function $G(r, r_0, \omega)$ represents the wave amplitude induced by a force F_0 (of unit strength) acting continuously at a source point r_0 with driving frequency ω and $\mu(r)$ denotes the mass density. The wave

energy density induced by the source is

$$\varepsilon_{r_0}(r, \omega) \propto \mu \omega^2 |G(r, r_0, \omega)|^2. \quad (3)$$

The bulk of the literature in acoustics and vibrational dynamics continues at this point by expanding the Green function in terms of eigenfunctions of either the full system or its subcomponents. We propose to follow a different route here by introducing a connection between the energy density and an underlying ray dynamics and expressing the Green function in terms of classical rays.

3.2. Small wavelength asymptotics of the Green function

The linear wave operator \hat{H} can in a natural way be associated with a ray dynamics via the Eikonal approximation. A brief overview introducing the method is given in Appendix A. In particular, a Hamilton function H related to the operator \hat{H} is obtained, typically by replacing $i\nabla \rightarrow p$, see for example (A.2); here, p is referred to as ‘momentum variable’ in the context of Hamiltonian mechanics and is equivalent to a local wavenumber.

Using small wavelength asymptotics, one can write the Green function $G(r, r_0, \omega)$ solving Eq. (2) as sum over *all* classical rays going from r_0 to r for fixed $H(r, p) = \omega^2$, where H is again the Hamilton function associated with the operator \hat{H} and p is the wavenumber. One obtains [29]

$$G(r, r_0, \omega) = C \sum_{j: r \rightarrow r_0} A_j e^{iS_j(\omega) - iv_j \pi/2}, \quad (4)$$

with prefactor

$$C = \frac{F_0 \pi}{\mu(r_0) \omega} \frac{1}{(2\pi i)^{(d+1)/2}},$$

where $d = 1, 2$ or 3 is the space dimension. The action $S_j(\omega)$ is defined in Eq. (A.4), and is usually the dominant ω dependent term; for example, for pressure waves in homogeneous media, one obtains a phase term $S = |p|L = \omega L/c$ where L is the distance between source and receiver point. The amplitudes A_j can be written in the form [27,30]

$$A_j = A_j^{(d)} A_j^{(c)} A_j^{(g)} \quad (5)$$

containing contributions due to damping (d), conversion and transmission/reflection coefficients (c) and geometrical factors (g). The damping factor is typically of the form $A_j^{(d)} = \exp(-\alpha_j L_j)$ with α_j , the damping rate and L_j , the geometric length of the trajectory. Furthermore, $A_j^{(c)}$ corresponds to the product of reflection, transmission or mode conversion amplitudes encountered by the trajectory j at boundaries or material interfaces [5,11,31–34]. Finally, $A_j^{(g)}$ contains geometric information and is of the form

$$|A_j^{(g)}|^2 = \frac{1}{|\dot{r}||\dot{r}_0|} \left| \frac{\partial^2 S}{\partial r^\perp \partial r_0^\perp} \right|, \quad (6)$$

where $|\cdot| = |\det(\cdot)|$ and the derivatives are taken in a local coordinate system r^\perp, r_0^\perp perpendicular to the trajectory at the initial and final point. The phase index v_j contains contributions from transmission/reflection coefficients at interfaces and from caustics, that is, singularities in the amplitude in Eq. (6). Furthermore, \dot{r}_0, \dot{r} denote the ‘ray-velocities’ at the start and endpoint with respect to a ‘fictitious’ time introduced in Appendix A.

The representation (4) has been considered in detail in quantum mechanics, see the books by Gutzwiller [29], Stöckmann [35] and Haake [36]. It is valid also for general wave equations in elasticity such as the biharmonic [34] and the Navier–Cauchy equation [27]; in the latter case, G becomes matrix valued. Note that the summation in Eq. (4) is typically over infinitely many terms where the number of contributing rays increase (in general) exponentially with the length of the trajectories included. This gives rise to convergence issues, especially in the case of low or no damping, see [11] and references therein.

The wave energy density, Eq. (3), can now be expressed as a double sum over classical trajectories, that is,

$$\begin{aligned} \varepsilon_{r_0}(r, \omega) &\propto \sum_{j, j': r_0 \rightarrow r} A_j A_{j'} e^{i(S_j - S_{j'} - (v_j - v_{j'})\pi/2)} \\ &= \rho(r, r_0, \omega) + \text{off-diagonal terms.} \end{aligned} \tag{7}$$

The dominant contributions to the double sum arise from terms in which the phases cancel exactly; one thus splits the sum into a *diagonal part* $\rho(r, r_0, \omega)$ (which can be identified with a *phase space density* as shown below),

$$\rho(r, r_0, \omega) = \sum_{j: r_0 \rightarrow r} |A_j|^2 \tag{8}$$

containing only pairs with $j = j'$ in Eq. (7) and an *off-diagonal part* containing the rest. The diagonal contribution gives a smooth background signal, which is here proportional to the energy density; the off-diagonal terms give rise to fluctuations on the scale of the wavelength. The phases related to different trajectories are (largely) uncorrelated and the resulting net contributions to the off-diagonal part are in general small compared to the smooth part—especially when considering averaging over frequency intervals of a few wavenumbers. (There are exceptions from this general rule; length correlations between certain subsets of orbits can lead to important off-diagonal contributions. Coherent backscattering or action correlations between periodic rays which have been identified to explain the universality of random matrix statistics are examples thereof; see [11] for details.)

In what follows, we will focus on the diagonal part, that is, we will show that neglecting off-diagonal terms is equivalent to the standard ray-tracing approximation. We will show furthermore that ray tracing can be written in terms of linear phase space operators and that SEA can be derived as an approximation of these operator. The connection between SEA and classical (thermodynamical) flow equations is thus put on sound foundations and the validity of the basic SEA assumptions as outlined in Section 2 can be quantified.

4. Propagation of phase space densities—from ray tracing to SEA

4.1. Phase space operators and probability densities

We consider the situation of a source localised at a point r_0 emitting waves continuously at a fixed frequency ω . Standard ray-tracing techniques estimate the wave energy at a receiver point r by determining the density of rays starting in r_0 (within the constraint $H(r_0, p_0) = \omega^2$) and reaching r after some unspecified time. This can be written in the form

$$\rho(r, r_0, \omega) = \int_0^\infty d\tau \int dp \int dX' w(X', \tau) \delta(X - \varphi^\tau(X')) \rho_0(X'; \omega), \tag{9}$$

where $X = (p, r)$ denotes a point in *phase space*, (see Appendix A), and the initial density

$$\rho_0(X'; \omega) = \delta(r' - r_0) \delta(\omega^2 - H(X')) \tag{10}$$

is centred at the source point r_0 . Furthermore, $X(\tau) = \varphi^\tau(X')$ is the phase space flow generated by equations of motion of the form (A.3) with initial conditions $X(0) = X'$ and τ is the time introduced in Eq. (A.3). It can be shown that Eq. (9) is equivalent to the diagonal approximation, Eq. (8), see Appendix B.

The weight function $w(X, \tau)$ contains damping and reflection/transmission coefficients and we assume here that w is multiplicative, that is,

$$w(X, \tau_1) w(\varphi^{\tau_1}(X), \tau_2) = w(X, \tau_1 + \tau_2), \tag{11}$$

which is fulfilled for (standard) absorption mechanism and reflection processes. Note, that the integral kernel

$$\mathcal{L}^\tau(X, X') = w(X', \tau) \delta(X - \varphi^\tau(X')) \tag{12}$$

is a linear operator—often called the Perron–Frobenius operator—which (after setting $w = 1$) may be interpreted as a propagator for the Liouville equation describing the time evolution of phase space

densities [37]

$$\dot{\rho}(X) = \{H(X), \rho(X)\}$$

(where $\{\cdot, \cdot\}$ denotes the Poisson brackets) with solution

$$\rho(X, \tau) = \mathcal{L}^\tau[\rho_0] = \int dX' \delta(X - \varphi^\tau(X'))\rho_0(X').$$

Eq. (9) can be simplified to

$$\rho(r, r_0, \omega) = \int_0^\infty d\tau \int dp' w(p', r_0, \tau) \delta(r - \varphi_r^\tau(p', r_0)) \delta(\omega^2 - H(p', r_0)), \tag{13}$$

where $\varphi_r^\tau(X) = r(\tau)$ denotes the r -component of the flow vector. Eq. (13) is the starting point for a variety of ray-tracing techniques [5,6,8].

While the basic Eq. (13) may seem ‘obvious’ from a ray geometrical point of view, we provide in Section 3.2 and Appendix B a derivation from first principles starting from the wave equation. For references in a quantum context, see [38,39]. The connection between ray-tracing densities and the double sum over ray trajectories, Eq. (7), may form the basis for including ‘higher order’ wave effects contained in the off-diagonal part. In what follows, we will stay within the diagonal approximation, however.

4.2. Boundary maps and related operators

We will for simplicity assume that the wave problem is confined to a finite domain with well defined boundaries; we may, for example, consider the vibrations of (coupled) plates of finite size or acoustic/elastic problems within bodies of finite volume. The long time limit of the dynamics is then best described in terms of boundary maps, that is, one records only successive reflections of a ray trajectory at the boundary. We introduce a coordinate system on the boundary, $X_s = (s, p_s)$, where s parameterises the boundary and p_s denotes the momentum components tangential to the boundary at s (X_s is often referred to as Birkhoff coordinates). Phase space points $X = (r, p)$ on the boundary are mapped onto X_s by an invertible transformation $\mathcal{B} : X \rightarrow (X_s, \omega)$ with $H(X) = \omega^2$.

We now introduce two new operators: firstly, we define an operator \mathcal{L}_B propagating a source distribution from the interior to the boundary, that is,

$$\mathcal{L}_B(X_s, X') = w(X', \tau_B) \cos \theta \delta(X_s - \mathcal{B}(\varphi^{\tau_B}(X'))),$$

where X' is an arbitrary phase space point in the interior and $\tau_B(X')$ is the time it takes for a trajectory with initial condition X' to hit the boundary for the first time; the angle $\theta(X')$ is taken between the normal to the boundary at the point s and the incoming ray velocity vector p , see Fig. 1a. Secondly, we introduce the

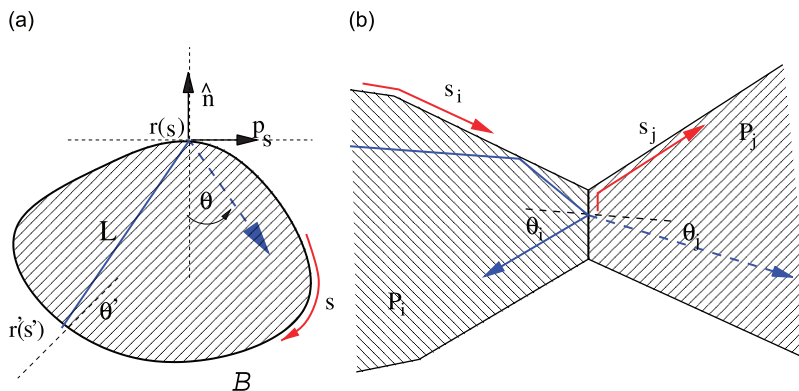


Fig. 1. Coordinates used for the boundary maps: (a) in case of a single subsystem and (b) at an intersection between two subsystems.

boundary operator

$$\mathcal{T}(X_s, X'_s; \omega) = w(X'_s)\delta(X_s - \phi_\omega(X'_s)),$$

which is the Perron–Frobenius operator for the boundary map

$$\phi_\omega(X'_s) = \mathcal{B}(\varphi^{\tau_B}(X')) \quad \text{with } X' = \mathcal{B}^{-1}(X'_s, \omega).$$

One can now write the stationary density in the interior, Eq. (13), in terms of the boundary operators introduced above. Firstly, the initial density (10) is mapped onto the boundary, that is, $\tilde{\rho}_0(X_s, \omega) = \int dX \mathcal{L}_B(X_s, X)\rho_0(X, \omega)$. The stationary density on the boundary induced by the initial boundary distribution $\tilde{\rho}_0(X_s, \omega)$ is then

$$\tilde{\rho}(\omega) = \sum_{n=0}^{\infty} \mathcal{T}^n(\omega)\tilde{\rho}_0(\omega) = (1 - \mathcal{T}(\omega))^{-1}\tilde{\rho}_0(\omega), \tag{14}$$

where \mathcal{T}^n contains trajectories undergoing n reflections at boundaries. The resulting density distribution on the boundary, $\tilde{\rho}(X_s, \omega)$, can now be mapped back into the interior using \mathcal{L}_B^{-1} and one obtains the density (13) after projecting down onto coordinate space, that is,

$$\rho(r, r_0, \omega) = \int dp dX_s \mathcal{L}_B^{-1}(X, X_s)\tilde{\rho}(X_s, \omega). \tag{15}$$

The long term dynamics is thus contained in the operator $(1 - \mathcal{T})^{-1}$ and standard properties of the Perron–Frobenius operators ensure that the sum over n in Eq. (14) converges for non-vanishing dissipation. Note, that for $w(X) \equiv 1$, \mathcal{T} has a largest eigenvalue 1 and the expression in Eq. (14) is singular. That is, in the case of no losses due to absorption or radiation, a source continuously emitting energy into the system will lead to a diverging energy density distribution in the long time limit. The eigenfunction of \mathcal{T} (and \mathcal{L}) corresponding to the eigenvalue 1 is the constant function; that is, for $w(X) \equiv 1$, the energy is equally distributed over the full phase space [40] in equilibrium.

To evaluate $(1 - \mathcal{T})^{-1}$ it is convenient to express the operator \mathcal{T} in a suitable set of basis functions defined on the boundary. Depending on the topology of the boundary, complete function sets such a Fourier basis for two-dimensional plates or spherical harmonics for bodies in three dimensions may be chosen. Denoting the orthonormal basis $\{\dots, \Psi_0, \Psi_1, \Psi_2, \dots\}$, we obtain

$$\begin{aligned} T_{nm} &= \int dX_s dX'_s \Psi_n^*(X_s) \mathcal{T}(X_s, X'_s; \omega) \Psi_m(X'_s) \\ &= \int dX'_s \Psi_n^*(\phi_\omega(X'_s))w(X'_s)\Psi_m(X'_s). \end{aligned} \tag{16}$$

The treatment is reminiscent to the Fourier-mode approximation in the WIA [13,14]; note, however, that the basis functions cover both momentum and position space here and can thus resolve spacial density inhomogeneities unlike WIA. If the boundary map $\phi_\omega(X_s)$ is not known or hard to obtain, it is often convenient to write the operator in terms of trajectories with fixed start and end points s' and s ; one obtains

$$\begin{aligned} T_{nm} &= \int ds ds' \frac{1}{|\partial s/\partial p'_s|} \Psi_n^*(X_s)w(X'_s)\Psi_m(X'_s) \\ &= \int ds ds' \left| \frac{\partial^2 S}{\partial s \partial s'} \right| \Psi_n^*(X_s)w(X'_s)\Psi_m(X'_s), \end{aligned} \tag{17}$$

with $X_s = (s, p_s(s, s'))$ and $X'_s = (s', p'_s(s, s'))$ and S is the action introduced in Eq. (A.4). The representation, Eq. (17), is advantageous for homogeneous problems where the ray trajectory connecting the points s' and s is a straight line, see the examples discussed in Section 5.

4.3. Subsystems

In many applications, it is natural to split the full system into subsystems and to consider the dynamics within each subsystem separately. Coupling between subelements can then be treated as losses in one

subsystem and source terms in the other. Typical subsystem boundaries are surfaces of reflection/transmission due to sudden changes in the material parameters or local boundary conditions (BC) due to for example bends in plates. Also, weakly connected subdomains such as two regions connected through small openings may be considered as separate subsystems. We denote the subsystems $\{P_1, \dots, P_N\}$ and describe the full dynamics in terms of the subsystem boundary operators \mathcal{T}^{ij} ; flow from P_j to P_i is possible only if the two subsystems are connected and one obtains

$$\mathcal{T}^{ij}(X_s^i, X_s^j) = w^{ij}(X_s^j)\delta(X_s^i - \phi_{\omega}^{ij}(X_s^j)), \quad (18)$$

where ϕ_{ω}^{ij} is the boundary map in subsystem j mapped onto the boundary of the adjacent subsystem i and X_s^i are the coordinates of subsystem i , see Fig. 1b. (Note, that subsystems exchanging wave energy are necessarily connected through a common boundary here.) The weight w^{ij} contains, among other factors, reflection and transmission coefficients characterising the coupling at the interface between P_j and P_i .

A basis function representation of the full operator T as suggested in Eq. (16) is now written in terms of subsystem boundary basis functions Ψ_n^i with

$$T_{nm}^{ij} = \int dX_s^i dX_s^j \Psi_n^{i*}(X_s^i) \mathcal{T}^{ij}(X_s^i, X_s^j) \Psi_m^j(X_s^j). \quad (19)$$

The equilibrium distribution on the boundaries of the subsystems is then obtained by solving the systems of equations (14)

$$(1 - T)\tilde{\rho} = \tilde{\rho}_0. \quad (20)$$

Here, T is the full operator including all subsystems and the equation is solved for the unknown energy densities $\tilde{\rho} = (\tilde{\rho}^1, \dots, \tilde{\rho}^N)$ where $\tilde{\rho}^i(n)$ denotes the (Fourier) coefficients of the density on the boundary of subsystem i . Equations similar to (20) have been considered by Craik [4] in the context of SEA. Note, that for a source localised in subsystem j , one obtains $\tilde{\rho}_0^i \neq 0$ only if P_i has a boundary in common with subsystem P_j .

4.4. From ray tracing to SEA

Up to now, the various representations given in Section 4 are all equivalent and correspond to a description of the wave dynamics in terms of the ray-tracing ansatz (9). Traditional ray tracing based on sampling ray solutions over the available phase space is rather inefficient, however. Convergence tends to be fairly slow, especially if absorption is low and long paths including multi-reflections need to be taken into account. Finding all the possible rays which connect a fixed source and receiver point is a computationally expensive boundary value problem and typically only a small sample of all the trajectories calculated are actually needed in determining the local energy density. In addition, the number of rays connecting source and receiver grows quickly (often exponentially) with the length of the ray trajectories setting fairly tight numerical bounds on the number of reflections one can take into account—a severe limitation in the low damping regime.

These problems are common for ray summation methods [11,37]. They can be overcome by describing the dynamics in terms of boundary operators and boundary functions Ψ_n as outlined above. While the representations are equivalent when employing the full set of basis functions (leading to infinite dimensional operators T), this is, of course, not the case for finite dimensional approximations. When considering the solutions of Eqs. (14) or (20), one is in general interested in smooth approximations of the energy density obtained from the classical flow. The resolution required is naturally limited by the wavelength of the underlying wave equation, but in many application a much coarser resolution will be sufficient. Convergence for obtaining such coarse grained energy density distributions is in general fast when increasing the dimension of the operators involved and often only a very small number of basis functions (of the order ≤ 10 per subsystem and momentum and position coordinate) are necessary. In addition, only short ray-segments are needed to evaluate operators of individual subsystems as multi-reflections are included explicitly in the sum (14).

An SEA treatment emerges when approximating the individual operators \mathcal{T}^{ij} in terms of the lowest order basis function (or Fourier mode), that is, the constant function $\Psi_0^j = (A_B^j)^{-1/2}$ with A_B^j , the area of the boundary of P_j . The matrix T^{ij} is then one-dimensional and gives the mean transmission rate from subsystem

P_j to P_i . It is thus equivalent to the coupling loss factor η_{ij} used in standard SEA equations, see Eq. (1). The resulting full N -dimensional T matrix (with N , the number of subsystems) yields a set of SEA equations using relation (20) (after mapping the boundary densities back into the interior with the help of local operators \mathcal{L}_B^i). Note, that the terms $E_i/n_i \sim \bar{\rho}^i$ in Eq. (1) are in fact mean energy densities as the mean density of eigenvalues n_i is to leading order proportional to A_i , the area/volume of subsystem P_i , which follows from Weyl's law [11].

The matrix T can in this approximation be interpreted as a transition matrix of an N -dimensional Markov chain; SEA is thus in fact a Markov approximation of a deterministic dynamics. Similar approaches have been taken in dynamical systems theory over the last decades leading to a stochastic interpretation of chaotic dynamical systems in terms of a thermodynamical formalism [37]. A Markov or SEA approximation is justified if the ray dynamics within each subsystem is sufficiently chaotic that a trajectory entering subsystem j 'forgets' everything about its past history before exciting P_j again. In other words, correlations within the dynamics must decay fast on the time scales of the staying time $\bar{\tau}_j$. This is the time scale it takes for a typical ray to leave P_j either by being transmitted to another subsystem P_i or by being lost due to absorption. In other words, the dynamics must equilibrate on the time scale $\bar{\tau}_j$. This condition will often be fulfilled if the subsystems' boundaries are sufficiently irregular, the subsystems are dynamically well separated and absorption and dissipation is small—conditions typically cited in an SEA context. In this case, SEA is an extremely efficient method compared to standard ray-tracing techniques. However, for subsystems with regular features, such as rectangular cavities or corridor-like elements, incoming rays are directly channelled into outgoing rays thus violating the equilibration hypothesis and introducing memory effects. Likewise, strong damping may lead to a significant decay of the signal before reaching the exit channel introducing geometric (system dependent) effects—that is, the distance between input and output channel becomes relevant.

These features can all be incorporated by including higher order basis functions for each subsystem boundary operator T^{ij} . This makes it possible to resolve the fine structure of the dynamics and its correlation as well as effects due to non-uniform damping over typical scales of the subsystem. As one increases the number of basis functions, a smooth interpolation from SEA to a full ray-tracing treatment is achieved. The maximal number of basis functions needed to reach convergence are expected to be relatively small thus making the new method more efficient than a full ray-tracing treatment—in particular in the small damping regime. Typical dimensions of T^{ij} are determined by escape-, correlation- and damping-rates of the ray dynamics in subsystem j . A priori or a posteriori bounds for the size of the basis set needed can thus be obtained from dynamical properties of the underlying ray flow.

Representing the ray dynamics in terms of finite dimensional transition matrices correspond to a refinement of an SEA technique. The new method takes advantage of the efficiencies of SEA, but includes additional information about the ray dynamics where necessary. It overcomes some of the limitations of SEA and puts the underlying SEA assumptions on sound foundations. We therefore refer to the new method as DEA stressing the importance of the dynamical properties of the underlying ray flow. Note that, like SEA and ray tracing, the method is purely based on a classical ray picture and is thus inherently a short wavelength approximation. It does not take into account wave-like phenomena; from a wave asymptotics point of view, these are contained in the off-diagonal contributions in Eq. (7). Wave effects often become important in mechanical structures containing elements with short and long wavelengths (at the same basic frequency) and hybrid SEA—finite element methods have been developed in this case [18,41,42]. An extension of these methods to DEA will be of importance, but is beyond the scope of this paper.

5. A numerical example: coupled two-plate systems

The method has been implemented numerically for a coupled two-plate system; the vibrational energy distribution has been calculated using DEA for plates of different shape where the coupling between the plates is achieved by choosing simply supported BC along a common line of intersection. We assume clamped BC at the outer edges, that is, Snell's law of reflection applies and no losses occur at the boundaries. The two plates have the same thickness and are homogeneous otherwise. The BC at the intersection introduces reflection and transmission and acts as a barrier thus providing a natural boundary for dividing the system into two distinct subsystems. Three different configurations are considered and shown in the insets of Fig. 2. Estimates for the

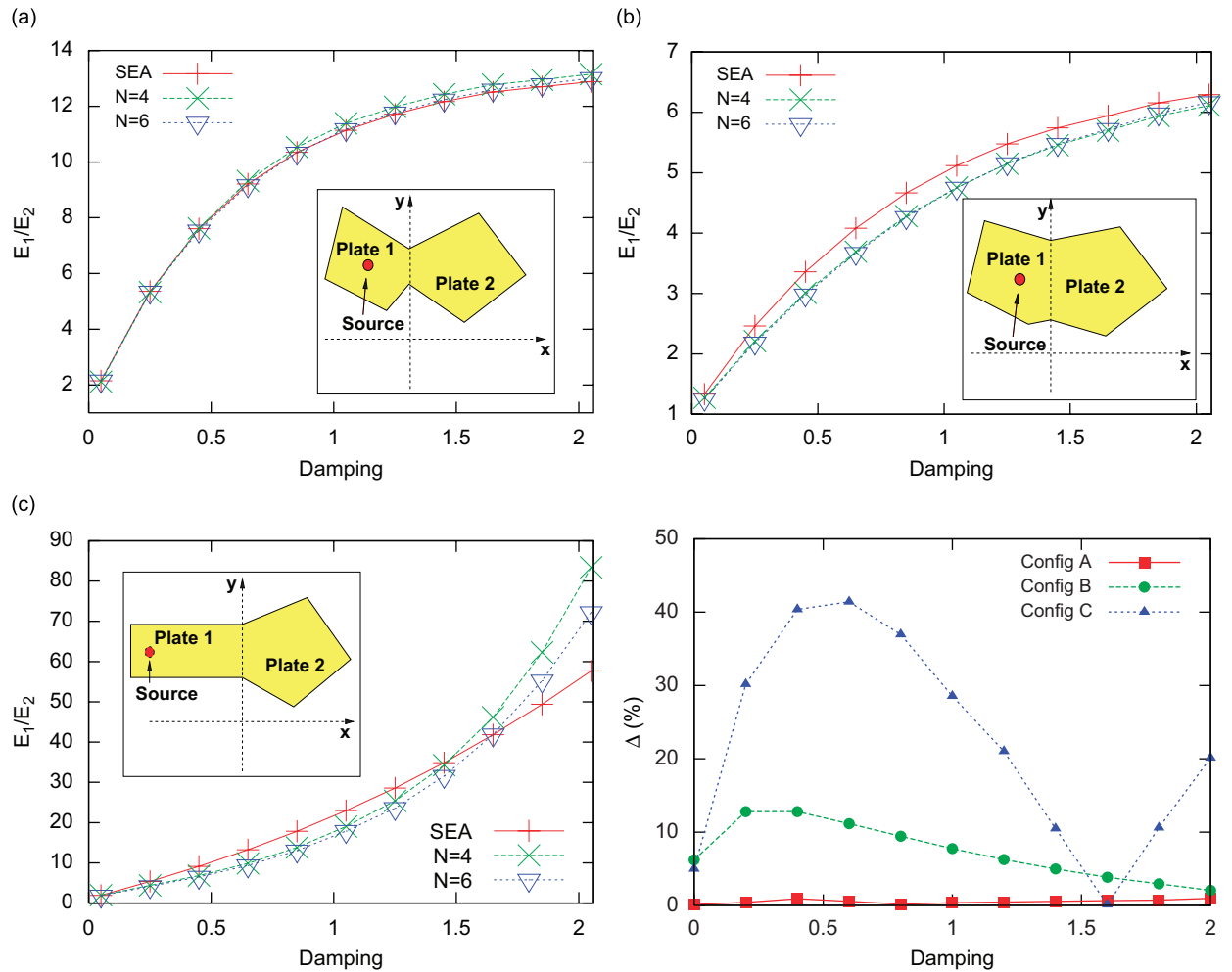


Fig. 2. Ratio of mean energy densities in plates 1 and 2 versus damping coefficient α for the three different plate geometries; lower right-hand corner: relative difference (in percent) between results from SEA ($N = 0$) and DEA with $N = 6$ for the three configurations (a–c).

vibrational energy induced by a point source in subsystem 1 will be obtain by using DEA and will be compared to standard SEA results.

5.1. Set-up

The plates are treated as two-dimensional systems and a Fourier basis both in position and momentum space is thus an adequate choice for the set of basis functions, that is

$$\Phi_n^i(s, p_s) = \frac{1}{\sqrt{2L_i}} e^{2\pi i(n_1 s/L_i + n_2 p_s/2)},$$

with $n = (n_1, n_2)$, integers, and $s \in [0, L_i], p_s \in (-1, 1)$, where L_i is the length of the boundary and $i = 1$ or 2. The wavenumber is set equal to 1 here. Note, that the estimates for the energy distributions obtained via DEA are frequency independent in this example as neither the ray paths nor the reflection coefficients at the ray splitting boundary depend on ω . We also assume for simplicity that the damping coefficient α is independent of the driving frequency. For a set of material parameters suitable for our model (and needed, for example, in a finite element calculation), see Table I in Ref. [43] from which one of the configurations—configuration B—has been taken. The transmission probability at the intersection of the

two plates yields for simply supported BC

$$w_t(\theta) = \frac{1}{2} \cos^2 \theta,$$

with $\theta \in [-\pi/2, \pi/2]$, the angle between the incoming ray and the normal to the surface.

Given the start and end point s^i, s^j on the boundary of either plate 1 or 2, one can obtain the rays, their lengths and the angles of intersection (and thus the momentum components tangential to the boundary) easily. The integral representation of the boundary operator in form (17) is thus advantageous. Writing out the Jacobian $|\partial s/\partial p'|$, one obtains

$$T_{nm}^{ij} = \int ds^i ds^j w^{ij} \frac{\cos \theta^i \cos \theta^j}{L(s^i, s^j)} \Phi_n^{i*} \Phi_m^j,$$

where $L(s^i, s^j)$ is the length of the trajectory. The weight function is given as

$$w^{ij} = w_b^{ij} e^{-\alpha L},$$

with α , the damping coefficient, and the reflection/transmission coefficients are

$$w_b^{ij}(s^i, s^j) = \begin{cases} \delta_{ij} & \text{if } s^i \notin B_I^j, \\ \delta_{ij} + (-1)_{ij}^\delta w_t(\theta^i(s^i, s^j)) & \text{if } s^i \in B_I^j, \end{cases}$$

where B_I^j denotes the part of the boundary in the coordinate system s^i lying on the intersection of plates 1 and 2.

5.2. Numerical results

The plates considered in this study all consist of sets of straight boundaries¹—such polygonal shapes are typical for many engineering applications. Three different set-ups have been chosen (see Fig. 2):

- *Configuration A* comprises two subsystems of irregular shape with a line of intersection relatively small compared to the total length of the boundaries; the two subsystems are thus well separated and SEA is expected to work well.
- *Configuration B* consists of two plates where the line of intersection is of the order of the size of the system; the only dynamical barrier is posed by the BC itself. The standard SEA assumption of weak coupling and a quasi-stationary distributions in each subsystem may thus be violated. (This configuration has also been studied in Refs. [19,43].)
- *Configuration C* has a left-hand plate with regular features and rays are channelled out of this plate effectively introducing long-range correlations in the dynamics thus again violating a typical SEA assumption. In addition, the source is positioned at the far end of plate 1 in contrast to the other two configurations with a source placed close to the intersection.

Note, that SEA results are in general insensitive to the position of the source, whereas actual trajectory calculations may well depend on the exact position especially for strong damping and for sources placed close to or far away from points of contact between subsections.

Numerical calculations have been done for finite basis sets up to $n_1, n_2 = -N, \dots, N$ with $N \leq 6$. This gives rise to matrices of the sizes $\dim T = 2(2N + 1)^2$ with basis functions covering position and momentum coordinates uniformly in both subsystems. Energy distributions have been studied as a function of the damping rate α . Note, that in the limit $\alpha \rightarrow 0$, the matrix T has an eigenvalue one with eigenvector corresponding to an equidistributed energy density over both plates, see the discussion following Eq. (15). In the case of no damping, the ray dynamics explores the full phase space uniformly on the manifold $H(X) = \omega^2$ in the long time limit. Eq. (20) is singular for $\alpha = 0$ and the solutions become independent of the source

¹To be precise, polygonal shapes as considered here lead to pseudo-integrable dynamics which is strictly speaking not even ergodic; at the level of approximation considered here, the decay of correlation in the dynamics of irregular polygons is sufficient in principle to test the SEA assumptions.

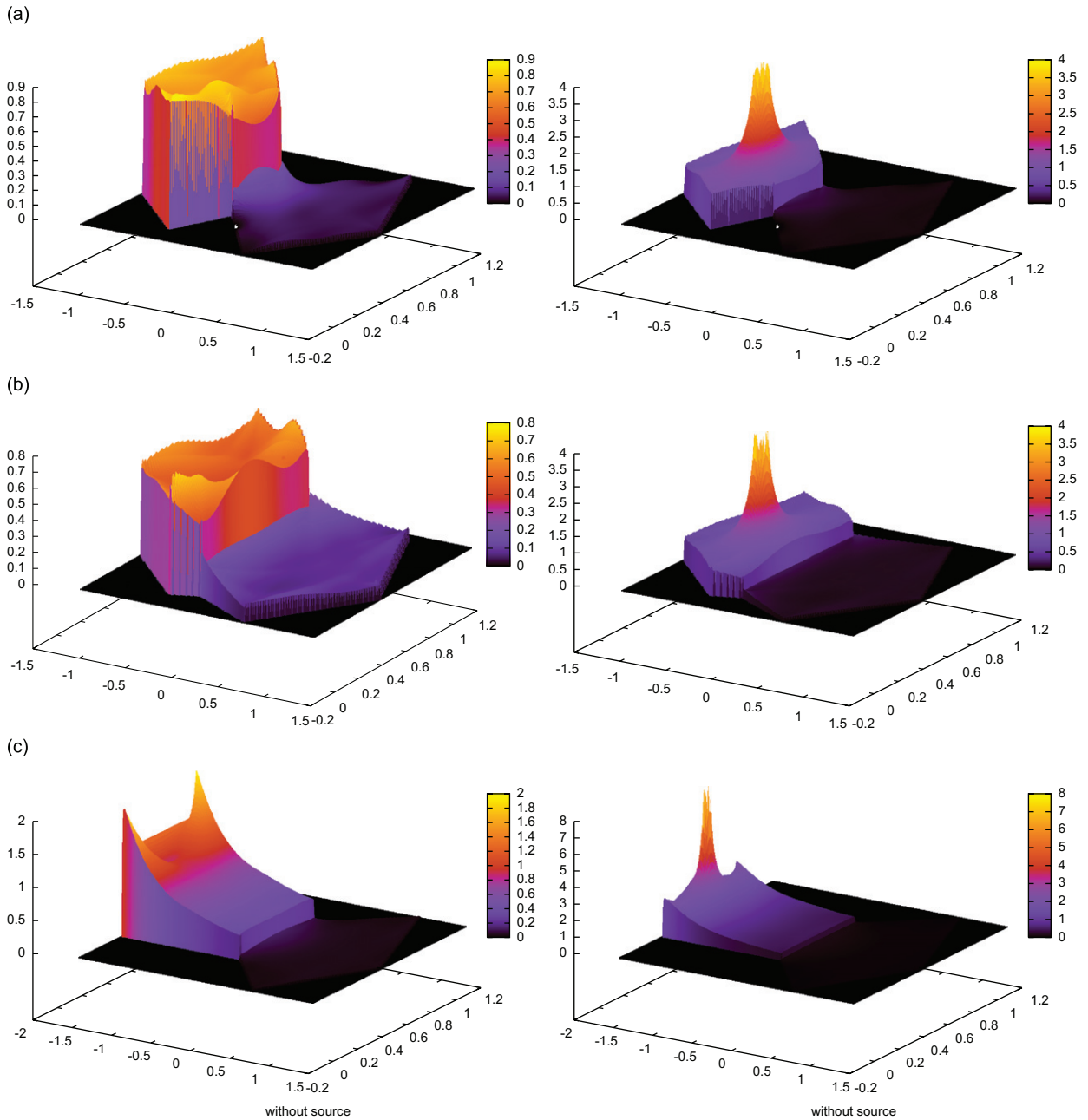


Fig. 3. Energy density distributions for the three configurations (a–c) for $\alpha = 1$ and $N = 6$; left: wave energy induced by reflections from the boundary; right: total wave energy distribution including direct contributions from the source.

distribution ρ_0 for $\alpha \rightarrow 0$. One obtains

$$\lim_{\alpha \rightarrow 0} \bar{\rho}_1 = \lim_{\alpha \rightarrow 0} \frac{\varepsilon_1}{\varepsilon_2} = 1,$$

where $\bar{\rho}_i$ denotes the mean ray density in plate i averaged over the area of the plate and ε_i is the corresponding mean energy density obtained from Eq. (3).

Results for the relative energy density distribution for the two-plate systems are shown in Fig. 2. Increasing the basis size—indicated here by the index N —leads to fast convergence as is evident from the figures.

An SEA-like treatment corresponds to $N = 0$, here. The lower right-hand panel in Fig. 2 also shows the difference between an SEA and DEA treatment (the latter with $N = 6$).

SEA works remarkably well for configuration A, for which the main SEA assumptions, that is, irregular shape, well separated subsystems and relative small damping, are fulfilled. The deviations between SEA and the high-resolution result $N = 6$ are of the order of a few percent. Given that SEA describes the energy densities here in terms of a system of only two coupled equations, this clearly shows the power of SEA compared to, for example, ray-tracing methods. In configuration B, the division into two subsystems is less clear-cut and deviations from SEA due to the strong coupling between the plates may be expected. Indeed, one finds a higher energy density in plate 2 than expected from SEA—energy dissipates into plate 2 before an equilibrium distribution is attained in plate 1. The effect is here of the order of 10% and thus still relatively small.

However, it is not too difficult to devise plate configurations where significant deviations from SEA occur. In configuration C, plate 1 has a rectangular shape thus acting as an effective channel for transporting wave energy from plate 1 to plate 2; the plate shape thus induces long range correlations and memory effects into the ray dynamics. In addition, the source has been placed away from the intersection magnifying both the influence of correlation effects as well as short range effects due to absorption for large α . One indeed finds more wave energy in plate 2 than expected from an SEA treatment for small α —a clear sign that plate 1 acts as an effective channel. For large α , however, the wave energy gets damped out before reaching the intersection due to the relative long path lengths caused by the position of the source. Thus, less wave energy than expected from an SEA treatment reaches plate 2 and the ratio $\varepsilon_1/\varepsilon_2$ is above the SEA curve. Note, that the deviations between DEA and SEA are now significant and in the region of about 50%.

DEA makes it possible to resolve the wave intensity distribution within each of the subsystems. The boundary distribution obtained from Eqs. (14) and (15) can be mapped back into the interior using the operator \mathcal{L}_B^{-1} in each subsystems, see Eq. (15). The spatial resolution of the wave energy density contains important information about, for example, the (acoustic) radiation characteristics of subelements in the high-frequency limit. In Fig. 3, typical intensity distributions are shown for the three plate configurations at a medium damping rate $\alpha = 1$ and $N = 6$. The left-hand panel shows the wave distribution induced by rays reflected from the boundary (indirect contributions), the right-hand panel also includes the direct rays emanating from the source point. (It is worth clarifying that only the indirect signals have been considered in the results presented in Fig. 2). The wave intensity plots confirm the observations described earlier; while for configurations A and B, one can identify a quasi-equilibrium distribution in each subsystem characterised by a plateau-structure in each of the two plates, the correlated dynamics in configuration C leads to a smooth decay of the signal within plate 1.

6. Conclusions

We have shown that ray-tracing methods and SEA are closely related and that the latter is indeed an approximation of the former by smoothing out the details of ray dynamics within individual subsystems. We propose a numerical technique which interpolates between SEA and full ray tracing by resolving the ray dynamics on a finer and finer scale. This is achieved by expressing the dynamics in terms of linear boundary operators and representing those in terms of a set of basis functions on the boundary. The resolution of the dynamics is now determined by the number of boundary functions taken into account.

We provide a derivation starting directly from a short wavelength approximation of the wave equation and leading all the way to setting up the basic DEA equations; we thus offer a step by step account of the approximations and simplifications made. The basic SEA assumptions can be tested systematically by relating them back to aspects of the ray dynamics. Furthermore, extending SEA to DEA enhances the range of applicability of an SEA-like treatment.

DEA and SEA are high-frequency methods, that is, they will give estimates for the energy density distribution in a regime not accessible to ‘numerically exact’ PDE solvers such as finite element methods (FEM). These become computationally too expensive for high frequencies (that is, for wave problems where typical wavelength are more than 1–2 orders of magnitude smaller than the typical system size). A finite element analysis leads then to matrix equations too big to handle even for the supercomputer architectures

available today. SEA has thus become a valued alternative widely used in the engineering community for estimating energy distributions in wave problems with high-frequency noise sources. DEA is expected to give good results also only in the high-frequency limit; it will offer more robust and reliable estimates in this regime compared to SEA and may thus form the basis of a high-frequency black-box tool.

Neither SEA nor DEA are suitable to tackle so-called *mid-frequency problems*—that is, structures with a large variation in local wavelengths. These problems are common in engineering, but pose a serious challenge for modelling efforts, as they are in general also too hard to tackle by numerical methods such as FEM. SEA has been used as a starting point for penetrating the mid-frequency regime by employing hybrid methods based on combining FEM and SEA treatments [18,41,42,44]. Future efforts will be devoted to develop similar hybrid approaches for the new DEA approach, thus contributing to the development of stable and universal numerical modelling algorithms in the mid- to high-frequency range.

Acknowledgements

The author would like to thank Oscar Bandtlow, Brian Mace and Anand Thite for stimulating discussions, Stephen Creagh for suggestions and carefully reading the manuscript and Stewart McWilliam for providing some important references. Support from the EPSRC through a *Springboard fellowship* is gratefully acknowledged.

Appendix A. Ray dynamics

A ray or classical dynamics associated with a wave equation (2) can be obtained via the Eikonal approximation writing the solutions in the form of a phase $S(r)$ and amplitude $A(r)$; assuming that the amplitude A changes slowly on the scale of the wavelength, one obtains a governing equations for the phase S alone. For example, for the Helmholtz equation with $\hat{H} = c^2 \nabla^2$, one obtains

$$c^2(\nabla S)^2 = \omega^2, \quad (\text{A.1})$$

where c denotes the wave velocity (assumed to be constant here). Dissipative terms are usually incorporated in the equation for the amplitude A . The Hamilton–Jacobi equation (A.1) can be solved by the method of characteristics. After defining $p \equiv \nabla S$ (where we adopt the notation of classical mechanics where p refers to *momentum*) and the Hamilton function

$$H(p, r) = c^2 p^2 = \omega^2, \quad (\text{A.2})$$

one obtains the ray-trajectories $(r(\tau), p(\tau))$ from Hamilton's equations

$$\dot{r} = \frac{d}{d\tau} r = \nabla_p H = 2c^2 p; \quad \dot{p} = \frac{d}{d\tau} p = -\nabla_r H. \quad (\text{A.3})$$

The fictitious time τ is conjugated to the 'energy' ω^2 and is related to the physical time by $t = 2\omega\tau$. The dimensionless *action* S is given as

$$S(r, r_0) = \int_{r_0}^r dr' p(r'), \quad (\text{A.4})$$

where the integration is taken along a ray from r_0 to r on the manifold $H(r, p) = \omega^2$. For homogeneous media with constant wave velocity, as considered here, one obtains $S = |p|L$ with $L(r, r_0)$, the length of the ray path from $r_0 \rightarrow r$.

The ray dynamics in mechanical structures consisting of coupled subsystems will typically entail reflection on boundaries, partial reflection/transmission at interfaces between two media and multi-component ray dynamics including mode conversion. The latter may occur between pressure and shear 'rays' at boundaries for typical BC (such as free boundaries); note, that the different wave components have different local wave velocities and will thus follow different equations of motion (A.3).

The number of rays starting in r_0 (with arbitrary momentum) and passing through r increases (for fixed ω) rapidly with the length or the action of the ray trajectories. If the ray dynamics is chaotic, that is, the ray

solutions show exponential sensitivity to initial conditions, one finds that the number of trajectories going from $r_0 \rightarrow r$ increases exponentially with their length [29]. Regular dynamics such as the solution of Eq. (A.3) for rectangular or circular geometries leads to a power law increase in the number of ray solutions from $r_0 \rightarrow r$.

Appendix B. Derivation of the ray-tracing equation (9)

It will be shown here that Eq. (8) is equivalent to the ray tracing equations (9), (13). For further details on the derivation, see also Ref. [29]. Starting point is Eq. (13) (where we set $w \equiv 1$ here to simplify the notation), that is,

$$\rho(r, r_0, \omega) = \int_0^\infty d\tau \int dp' \delta(r - \varphi_r^\tau(p', r_0)) \delta(\omega^2 - H(p', r_0)). \tag{B.1}$$

We write the δ -functions in the form

$$\delta(r - \varphi_r^\tau(p', r_0)) \delta(\omega^2 - H(p', r_0)) = \sum_j \frac{1}{D} \delta(\tau - \tau_j) \delta(p' - p'_j), \tag{B.2}$$

where the index j counts all possible solutions of

$$\varphi_r^{\tau_j}(p'_j, r_0) = r; \quad H(p'_j, r_0) = \omega^2.$$

These are the rays emanating from the source point r_0 and reaching the final point r on the manifold $H = \omega^2$. The Jacobian D is

$$D = \frac{\left| \frac{\partial(r, H)}{\partial(p', t)} \right|}{\left| \frac{\partial(r, H)}{\partial(t)} \right|} = \begin{vmatrix} \frac{\partial r}{\partial p'} & \frac{\partial H}{\partial p'} \\ \frac{\partial r}{\partial t} & \frac{\partial H}{\partial t} \end{vmatrix}.$$

Making use of the equation of motion (A.3), one identifies $\partial H / \partial p' = \dot{r}'$ and we have $\partial H / \partial t = 0$. It is now convenient to switch to a local coordinate systems $r = (r_\parallel, r_\perp)$; $p = (p_\parallel, p_\perp)$ at the initial and final point where r_\parallel, p_\parallel point along the trajectory in phase space. One obtains

$$D = \begin{vmatrix} & & \dot{r}'_\parallel & \\ & \frac{\partial r}{\partial p'} & 0 & \\ & & \vdots & \\ \dot{r}'_\parallel & 0 & \dots & 0 \end{vmatrix} = |\dot{r}'| |\dot{r}'| \left| \frac{\partial r_\perp}{\partial p_\perp} \right| = |A^{(g)}|^{-2}, \tag{B.3}$$

where $A^{(g)}$ is the geometric contribution to the wave amplitude, Eq. (6). Combining Eqs. (B.2) and (B.3) with (B.1), one obtains the diagonal term (8).

References

[1] R.H. Lyon, Statistical analysis of power injection and response in structures and rooms, *Journal of the Acoustical Society of America* 45 (1969) 545.
 [2] R.H. Lyon, R.G. DeJong, *Theory and Application of Statistical Energy Analysis*, second ed., Butterworth-Heinemann, Boston, MA, 1995.
 [3] A.J. Keane, W.G. Price, *Statistical Energy Analysis*, Cambridge University Press, Cambridge, 1994 (see also Philosophical Transactions of the Royal Society of London A 346).
 [4] R.J.M. Craik, *Sound Transmission Through Buildings: Using Statistical Energy Analysis*, Gower, Hampshire, 1996.
 [5] H. Kuttruff, *Room Acoustics*, fourth ed., Spon Press, London, 2000.
 [6] V. Cervený, *Seismic Ray Theory*, Cambridge University Press, Cambridge, 2001.
 [7] J.W. Mc Kown, R.L. Hamilton Jr., Ray tracing as a design tool for radio networks, *IEEE Network Magazine* 27 (1991).

- [8] A.S. Glasser (Ed.), *An Introduction to Ray Tracing*, Academic Press, New York, 1989.
- [9] K.-S. Chae, J.-G. Ih, Prediction of vibrational energy distribution in the thin plate at high-frequency bands by using the ray tracing method, *Journal of Sound and Vibration* 240 (2001) 263.
- [10] S. Kulkarni, F.G. Leppington, E.G. Broadbent, Vibrations in several interconnected regions: a comparison of SEA, ray theory and numerical results, *Wave Motion* 33 (2001) 79.
- [11] G. Tanner, N. Søndergaard, Wave chaos in acoustics and elasticity, *Journal of Physics A* 40 (2007) R443.
- [12] K.H. Heron, Advanced statistical energy analysis, *Philosophical Transactions of the Royal Society of London A* 346 (1994) 501 see also [3].
- [13] R.S. Langley, A wave intensity technique for the analysis of high frequency vibrations, *Journal of Sound and Vibration* 159 (1992) 483.
- [14] R.S. Langley, A.N. Bercin, Wave intensity analysis of high frequency vibrations, *Philosophical Transactions of the Royal Society of London A* 346 (1994) 489 see also [3] p. 59.
- [15] A. Le Bot, A vibroacoustic model for high frequency analysis, *Journal of Sound and Vibration* 211 (1998) 537.
- [16] A. Le Bot, Energy transfer for high frequencies in built-up structures, *Journal of Sound and Vibration* 250 (2002) 247.
- [17] A. Le Bot, Derivation of statistical energy analysis from radiative exchanges, *Journal of Sound and Vibration* 300 (2007) 763.
- [18] B.R. Mace, P.J. Shorter, Energy flow models from finite element analysis, *Journal of Sound and Vibration* 233 (2000) 369.
- [19] B.R. Mace, Statistical energy analysis, energy distribution models and system modes, *Journal of Sound and Vibration* 264 (2003) 391; B.R. Mace, Statistical energy analysis: coupling loss factors, indirect coupling and system modes, *Journal of Sound and Vibration* 279 (2005) 141.
- [20] R.S. Langley, A derivation of the coupling loss factors used in statistical energy analysis, *Journal of Sound and Vibration* 141 (1990) 207.
- [21] T. Guhr, A. Müller-Groeling, H.A. Weidenmüller, Random-matrix theories in quantum physics: common concepts, *Physics Reports* 299 (1998) 189.
- [22] R.L. Weaver, On the ensemble variance of reverberation room transmission functions, the effect of spectral rigidity, *Journal of Sound and Vibration* 130 (1989) 487.
- [23] V. Cotoni, R.S. Langley, M.R.F. Kidner, Numerical and experimental validation of variance prediction in the statistical energy analysis of built-up systems, *Journal of Sound and Vibration* 288 (2005) 701.
- [24] R.S. Langley, A.W.M. Brown, The ensemble statistics of the energy of a random system subjected to harmonic excitation, *Journal of Sound and Vibration* 275 (2004) 823.
- [25] R.S. Langley, A.W.M. Brown, The ensemble statistics of the band-averaged energy of a random system, *Journal of Sound and Vibration* 275 (2004) 847.
- [26] R.S. Langley, V. Cotoni, Response variance prediction in the statistical energy analysis of built-up systems, *Journal of the Acoustical Society of America* 115 (2004) 706.
- [27] G. Tanner, N. Søndergaard, Short wave length approximation of a boundary integral operator for homogeneous and isotropic elastic bodies, *Physical Review E* 75 (2007) 036607.
- [28] N. Søndergaard, Moving frames applied to shell elasticity, *Journal of Physics A* 40 (2007) 5067.
- [29] M.C. Gutzwiller, *Chaos in Classical and Quantum Mechanics*, Springer, New York, 1990.
- [30] N. Søndergaard, G. Tanner, Wave chaos in the elastic disk, *Physical Review E* 66 (2002) 066211.
- [31] L. Cremer, M. Heckl, E.E. Ungar, *Structure-borne Sound*, second ed., Springer, Berlin, 1988.
- [32] R.S. Langley, K.H. Heron, Elastic wave transmission through plate/beam junctions, *Journal of Sound and Vibration* 143 (1990) 241.
- [33] R. Blümel, T.M. Antonsen Jr., B. Georgeot, E. Ott, R.E. Prange, Ray splitting and quantum chaos, *Physical Review Letters* 76 (1996) 2476.
- [34] E. Bogomolny, E. Hugues, Semiclassical theory of flexural vibrations of plates, *Physical Review E* 57 (1998) 5404.
- [35] H.-J. Stöckmann, *Quantum Chaos—An Introduction*, CUP, Cambridge, 1999.
- [36] F. Haake, *Quantum Signatures of Chaos*, second ed., Springer, Berlin, 2001.
- [37] P. Cvitanović, R. Artuso, P. Dahlqvist, R. Mainieri, G. Tanner, G. Vattay, N. Whelan, A. Wizba, *Chaos—classical and quantum*, 2008 (www.chaosbook.org).
- [38] B. Grammaticos, A. Voros, Semiclassical approximations for nuclear Hamiltonians. I. Spin-independent potentials, *Annals of Physics* 123 (1979) 359.
- [39] K. Richter, *Semiclassical Theory of Mesoscopic Quantum Systems*, Springer, Berlin, 2000.
- [40] R.L. Weaver, On diffuse waves in solid media, *Journal of the Acoustical Society of America* 71 (1982) 1608.
- [41] R.S. Langley, P. Bremner, A hybrid method for the vibration analysis of complex structural-acoustic systems, *Journal of the Acoustical Society of America* 105 (1999) 1657.
- [42] P.J. Shorter, R.S. Langley, Vibro-acoustic analysis of complex systems, *Journal of Sound and Vibration* 288 (2005) 669.
- [43] B.R. Mace, J. Rosenberger, The SEA of two coupled plates: an investigation into the effects of subsystem irregularity, *Journal of Sound and Vibration* 212 (1998) 395.
- [44] C.R. Fredö, A SEA-like approach for the derivation of energy flow coefficients with a finite element model, *Journal of Sound and Vibration* 199 (1997) 645.